68th International Astronautical Congress, Adelaide, Australia 25-29 September 2017.

IAC–17–C1.3.3

Monocular vision based simultaneous localization and mapping for close proximity navigation near an asteroid

Arunkumar Rathinam[a]*, Andrew G. Dempster [a]

[a] *Australian Centre for Space Engineering Research, School of Electrical Engineering and Telecommunications, UNSW Sydney, Australia, a.rathinam@student.unsw.edu.au*
* Corresponding author

Abstract

Missions to small celestial bodies are gaining interest in recent years and their mission profiles are evolving from scientific exploration and sample return missions to more advanced in-situ resource extraction and utilisation. This suggests the spacecraft operate more in the proximity of an asteroid than before, but the accuracies from ground-based navigation processes may not be sufficient. This highlights the need for autonomous on-board navigation techniques in future missions. To achieve an autonomous navigation, the spacecraft must be aware of its state and able to estimate the asteroid's state, geometry, and dynamic characteristics. The problem of navigation and mapping an unknown environment is interdependent and can be solved using the Simultaneous Localization and Mapping (SLAM) framework. This work proposes a visual SLAM framework for a spacecraft orbiting near an asteroid and estimates the unknown parameters through pose-graph optimization. This framework uses the registered images from the navigation camera and integrates both the spacecraft's motion and the rigid body dynamics of the asteroid, to estimate the relative pose of both spacecraft and asteroid, the asteroid's shape, and its dynamic characteristics. Experimental results from simulation suggest that the proposed method can accurately estimate the spacecraft's state, landmark position, and other unknown parameters.

Keywords: visual navigation, SLAM, asteroids, state estimation, factor graph

Nomenclature

$\mathbf{x}^i_{s,a}$	State at instance of time i, $\{i = 1, ..., N\}$, subscript s- spacecraft and a-asteroid
$\mathbf{r}$	position vector $\begin{bmatrix} x & y & z \end{bmatrix}'$
$\mathbf{q}$	quaternion $\begin{bmatrix} q_0 & q_x & q_y & q_z \end{bmatrix}'$
$\mathbf{v}$	velocity vector $\begin{bmatrix} v_x & v_y & v_z \end{bmatrix}'$
ω	angular velocity vector $\begin{bmatrix} \omega_x & \omega_y & \omega_z \end{bmatrix}'$
$\mathbf{l}^i_k$	measurement of landmark k, at instance i; k is the number of landmarks $\{k = 1, ..., M\}$
$\dot{r}, \dot{v}$	derivative of position & velocity
$\dot{q}, \dot{\omega}$	derivative of quaternion & angular velocity
J	inertia matrix
$W(q)$	quaternion rates matrix
Q_v, Q_ω	process noise model including disturbance forces, torques applied to the spacecraft
$\mathbf{r_c}$	vector from the spacecraft to the asteroids center of rotation
r_k	radius of the sphere formed by landmark k during asteroid rotation (scalar value)
μ	standard gravitational parameter

Acronyms/Abbreviations

SCB - Small celestial body
EKF - Extended Kalman Filter
RBPF - Rao-Blackwellised Particle Filter
ICP - Iterative Closest Point
TAG - Touch-and-go

1. Introduction

Exploration missions to SCB in the past including NEAR Shoemaker, Stardust, Hayabusa, Rosetta, and Dawn are known for their scientific importance and enabled scientists to learn more about the formation and evolution of the solar system. OSIRIS-REx and Hayabusa-2 are two ongoing missions to explore asteroids and scheduled to reach their respective targets in 2018. Both missions are expected to perform a series of experiments near the asteroid and finally, bring samples back to Earth. Other than exploration missions, the concept of mining asteroids for resource extraction and utilisation to support long term space missions has gained interest in recent years. This trend is expected to grow in the future and the missions will demand more complex close proximity operations near the asteroid and this dictates the need for autonomous on-board navigation techniques.

The key attribute of a SCB is its weak gravitational force and it makes proximity navigation extremely difficult. However, it allows a longer timeline for characterization and a gradual descent to the target during TAG manoeuvres. NEAR and Hayabusa successfully demonstrated landing on the asteroid with ground control at tens of meters of accuracy. However, future landings may require accuracies less than 5m because of either the lack of safe

landing spots at larger scales, or to target very specific regions for science [1]. Earlier research includes [2], [3], [4], [5] which were carried out to enable autonomous navigation near an asteroid. To operate autonomously in close proximity of an asteroid, the primary information that spacecraft needs is its position, orientation, and velocity (together termed as *pose or state*) . The spacecraft should also be aware of the *asteroid's pose* to perform relative navigation, together with its geometric shape and dynamic characteristics. The problem of navigation and mapping an unknown environment is interdependent and can be solved using a typical SLAM framework.

Most widely used SLAM approaches are based on the EKF which calculates a Gaussian posterior over the position of the robot as well as the detected landmarks. In the EKF, as the number of landmarks observed grows over time, maintaining a Gaussian posterior imposes a significant burden and the filter can become unstable due to the quadratic nature of the map [6]. Other popular SLAM approaches include particle filters [7], information filters [8] and graph-based SLAM [9].

1.1 Related works

In recent years, SLAM-based state estimation approaches were investigated for different mission applications. Particle filter based SLAM in [10] are used to estimate the pose and shape of a non-cooperating object. In [11], a Kalman filter and ICP are employed to estimate the state of the target objects for automated rendezvous and docking in on-orbit servicing applications. A RBPF-SLAM approach was presented in [12], to estimate the pose and attitude of a spacecraft maneuvering near an asteroid. Though particle filters have the advantage of efficient integration of the nonlinear measurement and motion models, the results suggest that the stability and precision of the RBPF-SLAM approach depend on the careful selection of parameters such as the number of particles, observation errors, etc. In another case [13], an EKF was implemented to track the spacecraft position and velocity (using co-state representation) and it used orbital dynamics to resolve scale. An EKF SLAM based approach was studied in [14], to predict the spin state estimation of a tumbling SCB and estimated the parameters including spacecraft position, orientation, and velocity, along with the target body mass, angular velocity and diagonal moment of inertia.

This work proposes a visual SLAM framework for a spacecraft orbiting near an asteroid and estimates the unknown parameters through pose-graph optimization. This work targets an asteroid rotating on its principal axis and assumes that the spacecraft orbits at a defined altitude similar to the characterization phase of a mission. This framework uses only the registered images from the navigation camera to extract the landmarks measurements and does not integrate the additional data (from inertial or attitude sensors). The initial state of the spacecraft and the asteroid are estimated through the least squares approach by solving the landmark measurements. Once initialised, this framework considers both the spacecraft's motion and the rigid body dynamics of the asteroid to predict the states and their corresponding measurements factors are recorded and solved to estimate landmark position, state of asteroid and the spacecraft.

2. Models

2.1 Dynamics of Spacecraft

The pose of the spacecraft at time instance i is denoted by $\mathbf{x}_s^i$, includes position $\mathbf{r}$, orientation $\mathbf{q}$ represented as quaternion, linear $\mathbf{v}$ and angular velocity ω.

$$\mathbf{x}_i = \begin{bmatrix} r & q & v & \omega \end{bmatrix}' \quad [1]$$

The spacecraft is assumed to be orbiting around the asteroid and the motion of the satellite is given by the dynamic equations below.

$$\dot{r} = v_s \quad [2]$$

$$\dot{q} = \frac{1}{2} W(q_s)^\top \omega_s \quad [3]$$

where quaternion rates matrix $W : \mathbb{H} \to \mathbb{R}^{3\times 4}$

$$W(q) = \begin{bmatrix} -q_x & q_0 & -q_z & q_y \\ -q_y & q_z & q_0 & -q_x \\ -q_z & -q_y & q_x & q_0 \end{bmatrix}$$

$$\dot{v} = \frac{-\mu}{\|r^3\|}\mathbf{r} + Q_{vs} \quad [4]$$

$$\dot{\omega} = -J^{-1}[\omega\times]J\omega_s + Q_{\omega s} \quad [5]$$

where,

$$[\omega\times] = \begin{bmatrix} 0 & -\omega_z & \omega_y \\ \omega_z & 0 & -\omega_x \\ -\omega_y & \omega_x & 0 \end{bmatrix}$$

2.2 Dynamics of the asteroid

The asteroid is assumed to be rotating on its principal axis and follows rigid body dynamics. The asteroid's state is represented similarly to the spacecraft's state with a 13 state vector $\mathbf{x}_a^i$. The derivative of the state is presented below,

$$\dot{r} = v_a \quad [6]$$

where $v \sim 0$

$$\dot{q} = \frac{1}{2} W(q_a)^\top \omega_a \quad [7]$$

$$\dot{v} = Q_{va} \quad [8]$$

where Q_{va} is assumed to be very small disturbance force

$$\dot{\omega} = -J^{-1}\left[\omega\times\right] J\omega_a + Q_{\omega a} \quad [9]$$

3. Framework

3.1 Initialization

In SLAM, good initialization helps with faster convergence as well as minimise the risk of convergence to local minima[15]. Our current framework targets a rotating asteroid, so we propose an initialization based on the least square approach. We followed the model presented in [16], to estimate the average center of rotation. The cost function of the least squares approach is given below.

$$C = \sum_{k=1}^{M} \sum_{i=1}^{N} \left[\left(\mathbf{l}_k^i - \mathbf{r}_c \right)^2 - \left(r_k \right)^2 \right]^2 \qquad [10]$$

The landmark measurements $\mathbf{l}_k^i$ from the spacecraft at two subsequent timeframes i are used to estimate the center of rotation $\mathbf{r_c}$ of the asteroid.

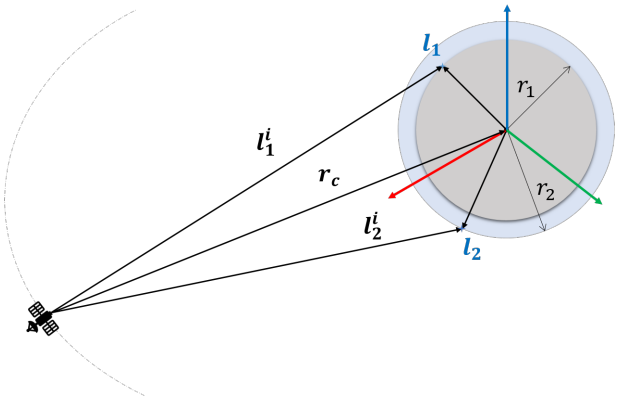

Fig. 1: Depicition of rotating asteroid with landmark and measurements from the spacecraft

To minimise the cost function, we need to estimate r_k and $\mathbf{r}_c$. We can derive r_k interms of $\mathbf{r}_c$ by differentiating the cost function w.r.t. r_k and it results in the equation below.

$$r_k = \sqrt{\frac{1}{N} \sum_{i=1}^{N} \left(\mathbf{l}_k^i - \mathbf{r}_c \right)^2} \qquad [11]$$

The least square solution is of the form $Ax = \mathbf{b}$ and the solution can be derived as follows

$$A.\mathbf{r}_c = \mathbf{b} \qquad [12]$$

where,

$$A = 2 \sum_{k=1}^{M} \left[\left\{ \frac{1}{N} \sum_{i=1}^{N} \mathbf{l}_k^i (\mathbf{l}_k^i)^T \right\} - \overline{\mathbf{l}_k} \left(\overline{\mathbf{l}_k} \right)^T \right]$$

$$\mathbf{b} = \sum_{k=1}^{M} \left[\overline{(\mathbf{l}_k)^3} - \overline{\mathbf{l}_k} \overline{(\mathbf{l}_k)^2} \right]$$

$\overline{(\mathbf{l}_k)^3} = 1/N \sum_{i=1}^{N} \left(\mathbf{l}_k^i \right)^3$, $\overline{(\mathbf{l}_k)^2} = 1/N \sum_{i=1}^{N} \left(\mathbf{l}_k^i \right)^2$ and $\overline{(\mathbf{l}_k)} = 1/N \sum_{i=1}^{N} \left(\mathbf{l}_k^i \right)$

The estimate $\mathbf{r_c}$ obtained is in the spacecraft's reference frame and needs to be transformed to an inertial frame. Through the inverse transformation, the asteroid's center of rotation along with the initial landmark positions and the spacecraft's position are initialised in an inertial frame.

3.2 Formulation

3.2.1 Factor Graph

A factor graph is a type of probabilistic graphical model. It has two types of node, i.e., variable nodes and factor nodes. Variable nodes represent the state that we are interested in estimating (such as the state of the spacecraft, asteroid and its landmarks). Factor nodes represent the probability distribution between the two nodes and often represent the error between the two variables. $f(a, b)$ denotes the factor between the random variables a and b. An edge connects two nodes and the graph is bipartite i.e. an edge always joins a variable node to a factor node.

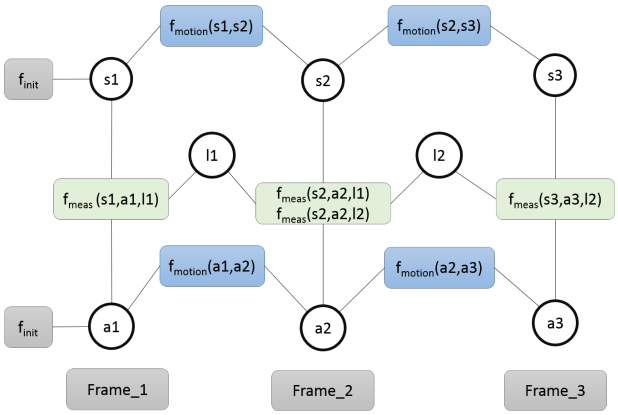

Fig. 2: Factor graph representation of the framework with *variables* (spacecraft state, landmark position, asteroid state) and *factors* (measurement and motion)

3.2.2 Method

The initial position of the spacecraft and asteroid are obtained from the least square approach and from the estimate we create the absolute factor nodes along with the landmark measurement factors in the graph. Following initialization, the solution updates for subsequent frames are done within the framework of factor graph SLAM. For the next frame, the spacecraft's state and the asteroid's state are propagated using the dynamic models over a defined time interval through RK4 integration and a small amount of perturbation is included through process noise models at every time step. At the end, new motion factors are added to the graph. The landmark measurements during each time instant is analysed, if the landmark is previously known, a new measurement factor is created with the state of the asteroid and spacecraft and added to the graph, if not (in case of new landmarks)

Algorithm 1 SLAM Framework

Initialization

$\{\mathbf{r}_c\} \leftarrow$ *estimateCoR* $\left\{\mathbf{l}_k^i\,(u,v,z)\right\}$

where u,v are pixel coordinates, z depth

$\left\{\mathbf{x}_a\,(\mathbf{r}_c)\,,\mathbf{l}_k^i,\mathbf{x}_s\right\} \leftarrow$ *invTransform* $\left\{\mathbf{r}_c,\mathbf{l}_k^i,\mathbf{x}_s\right\}$

$\left\{\mathbf{x}_a^1,\mathbf{l}_k^1,\mathbf{x}_s^1\right\} \leftarrow$ *initialize* $\left\{\mathbf{x}_a\,(\mathbf{r}_c)\,,\mathbf{l}_k^i,\mathbf{x}_s\right\}$

`Factor_graph` $\leftarrow$ *addFactors* $\left\{\mathbf{x}_a^1,\mathbf{l}_k^1,\mathbf{x}_s^1\right\}$

Prediction and Estimation

for $i = 2,...,N$ **do**

$\left\{\dot{\mathbf{x}}_a^i,\dot{\mathbf{x}}_s^i\right\} \leftarrow$ *predMotion* $\left\{\mathbf{x}_a^{i-1},\mathbf{x}_s^{i-1},dt\right\}$

`Factor_graph` $\leftarrow$ *addMotionFactor* $\left\{\dot{\mathbf{x}}_a^i,\dot{\mathbf{x}}_s^i\right\}$

if *newLandmarkFeature* **then**

`Factor_graph` $\leftarrow$ *initNewLmk* $\left\{\mathbf{l}_k^i\,(u,v,z)\right\}$

`Factor_graph` $\leftarrow$*addMeasFac*$\left\{\mathbf{l}_k^i,\dot{\mathbf{x}}_a^i,\dot{\mathbf{x}}_s^i\right\}$

else

`Factor_graph` $\leftarrow$ *addMeasFac*$\left\{\mathbf{l}_k^i,\dot{\mathbf{x}}_a^i,\dot{\mathbf{x}}_s^i\right\}$

end if

$\left\{\mathbf{x}_a^i,\mathbf{l}_k^i,\mathbf{x}_s^i\right\} \leftarrow$ *solveGraph* {`Factor_graph`}

end for

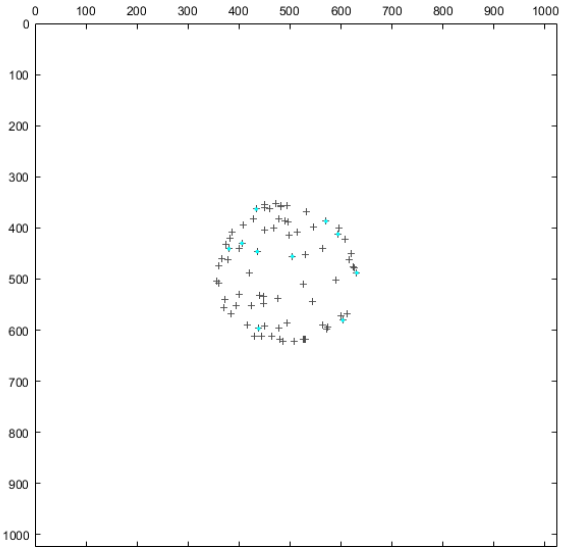

Fig. 4: View of landmarks from Navigation camera sensor frame with array size of 1024 x 1024 pixels

a new landmark is added to the landmark database and the new measurement factor is created and the graph is updated accordingly. The overall framework merges the state representations of the rigid body kinematics and dynamics of discrete-time with the pose graph representations. The optimization of unknown quantities to minimise the error is carried out efficiently by the QR factorization of sparse matrix.

4. Simulation

4.1 Setup

The Experimental setup is modeled in MATLAB and includes a simulated asteroid with approximately 200 distinct 3D landmark features randomly distributed on the asteroid's surface. The asteroid's diameter is set to be approx. 500 meters, with the landmark distribution varying between 480 $\sim$ 520 meters diameter. Next, the spacecraft is assumed to be orbiting at 600m radius from the center of the asteroid. The SLAM toolbox [17] was extended with the additional functionality to perform the simulations. The simulated model of the asteroid is shown in Fig. 3.

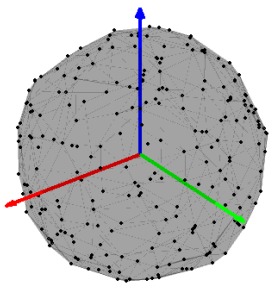

Fig. 3: Simulated asteroid model with landmarks

The camera is simulated with the focal length of 125mm which is comparable in focal length to navigation cameras used in similar SCB missions, which are between 125 $\sim$ 140mm. The navigation camera is assumed to be attached with the spacecraft and the position is known in spacecraft reference frame. The sensor array has 1024 x 1024 pixels, with a pixel size of 8.5 microns and gives the field of view of approx. 68°. The navigation camera captures the image as shown in Figure 4 and the pinhole camera model is used to compute the landmark positions from the image.

The rotational period of the asteroid is selected to be approx. 8hr or 3 spin/day as mentioned in [18]. The approximate angular velocity of the asteroid is

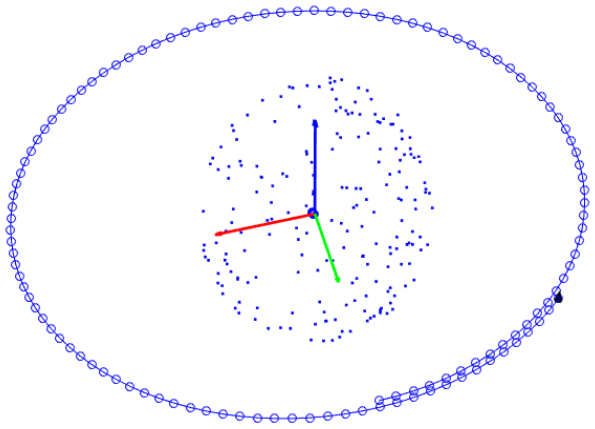

Fig. 5: Optimised landmarks position and spacecraft's position (represented as Key-frames) over the entire orbit through the factor graph approach

assumed to be known through light curve measurements from Earth. The spacecraft propagates its position at minute intervals and captures image at 10 min intervals to produce one keyframe in the graph. The observation error of the navigation camera was assumed to be zero mean and 0.5 pix STD and the altitude sensor depth error STD is 1m. The entire simulation covers a duration of about 120 keyframes, which is nearly 20 hours enough to revisit the landmarks on the surface of the asteroid 2∼3 times.

4.2 Results

The reconstructed shape of the asteroid with the landmark features is shown in Fig. 5. The reconstructed shape includes nearly 98% of the landmarks from the original landmark set. The mean error in landmark positions at every keyframe of the simulation is shown in Fig. 6. The mean error varies within ± 4 meters range and it is within the acceptable limits of future missions. Figure 7 shows the position errors for the landmarks that are visible for more than 10 keyframes in the simulation. Although both Fig. 6 and Fig.7 seem unconnected, detailed analysis suggests that the error tends to minimise after observing repeated landmarks in many frames . This is clearly seen after the region between 6 ∼ 8 Hr and 14 ∼ 16 Hr (where the number of repeated landmarks is minimum level), once the repeated landmarks are visible the error tends to converge. The above observation suggests well distributed landmarks across multiple timeframes can help reduce the error.

5. Conclusion

In this paper, a visual SLAM framework for a spacecraft orbiting near an asteroid is presented. Robust initialisation of state of asteroid, landmark position and spacecraft state is done through the least squares approach. The framework used only the landmark measurements and no external means of reference were integrated(such as inertial sensors or attitude sensors). Integrating the external reference is expected to further reduce error and improve state estimates. Reconstructing the shape of the asteroid based on the observed landmarks positions and the mean error in landmark positions is well within the accuracies demanded for future missions.

Future work includes expanding the framework to accommodate other unknown parameters in the estimation process and further relaxing the initial assumptions. Also, including images of the simulated 3D model and using image processing algorithms to match the features will test the robustness of the algorithm. Improvements in false data associations and landmark feature selection methods can also be examined. The computational efficiency of the process can be improved either to accommodate more landmarks or to implement the framework in realtime onboard the spacecraft.

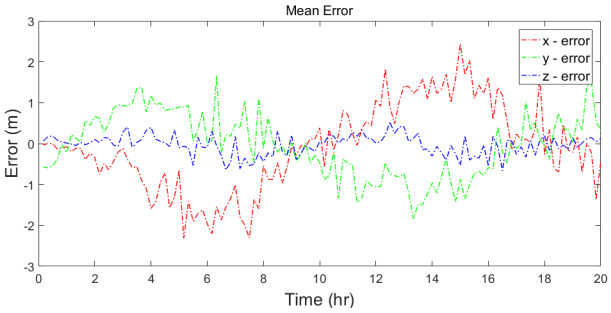

Fig. 6: Mean error of the landmarks over the entire time period

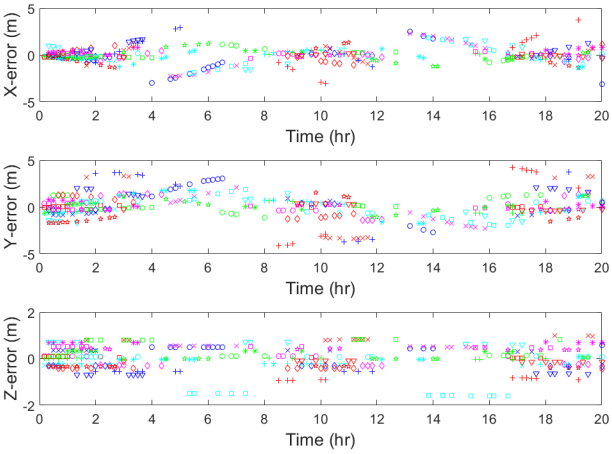

Fig. 7: Error plot for individual landmarks that are visible over more than 10 frames

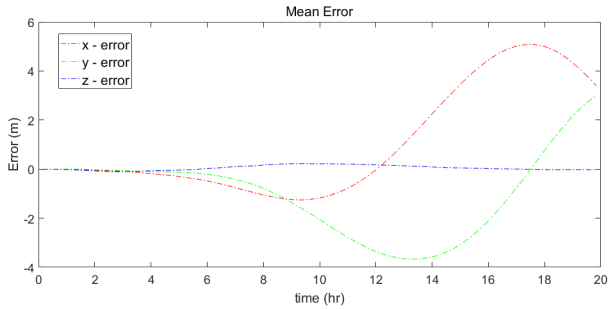

Fig. 8: Mean error of the spacecraft pose over the entire time period

References

[1] M. B. Quadrelli, L. J. Wood, J. E. Riedel, M. C. McHenry, M. Aung, *et al.*, "Guidance, navigation, and control technology assessment for future planetary science missions," *Journal of Guidance, Control, and Dynamics*, vol. 38, no. 7, pp. 1165–1186, 2015, ISSN: 0731-5090. DOI: 10.2514/1.G000525.

[2] J. Riedel, S Bhaskaran, S. Synnott, S. Desai, W. Bollman, *et al.*, "Navigation for the new millennium: Autonomous navigation for Deep-Space 1," in *Space Flight Dynamics*, vol. 403, 1997, p. 303.

[3] T. Miso, T. Hashimoto, and K. Ninomiya, "Optical guidance for autonomous landing of spacecraft," *IEEE Transactions on Aerospace and Electronic Systems*, vol. 35, no. 2, pp. 459–473, 1999, ISSN: 0018-9251. DOI: 10.1109/7.766929.

[4] T. Kubota, T. Hashimoto, S. Sawai, J. Kawaguchi, K. Ninomiya, *et al.*, "An autonomous navigation and guidance system for MUSES-C asteroid landing," *Acta Astronautica*, vol. 52, no. 2, pp. 125 –131, 2003, Selected Proceedings of the 4th IAA International conference on L ow Cost Planetary Missions, ISSN: 0094-5765. DOI: 10.1016/S0094-5765(02)00147-9.

[5] S. Bhaskaran, N. Mastrodemos, J. E. Riedel, and S. P. Synnott, "Optical Navigation for the STARDUST Wild 2 Encounter," in *18th International Symposium on Space Flight Dynamics*, ser. ESA Special Publication, vol. 548, 2004, p. 455.

[6] S. Thrun, W. Burgard, and D. Fox, *Probabilistic Robotics*. The MIT Press, 2005, ISBN: 0262201623.

[7] M. Montemerlo and S. Thrun, "FastSLAM 2.0," in *FastSLAM: A Scalable Method for the Simultaneous Localization and Mapping Problem in Robotics*. Berlin, Heidelberg: Springer Berlin Heidelberg, 2007, pp. 63–90, ISBN: 978-3-540-46402-0. DOI: 10.1007/978-3-540-46402-0_4.

[8] S. Thrun, Y. Liu, D. Koller, A. Y. Ng, Z. Ghahramani, *et al.*, "Simultaneous localization and mapping with sparse extended information filters," *The International Journal of Robotics Research*, vol. 23, no. 7-8, pp. 693–716, 2004.

[9] G Grisetti, R Kummerle, C Stachniss, and W Burgard, "A tutorial on graph-based SLAM," *IEEE Intelligent Transportation Systems Magazine*, vol. 2, no. 4, pp. 31–43, 2010. DOI: 10.1109/MITS.2010.939925.

[10] S. Augenstein and S. M. Rock, "Simultaneous estimation of target pose and 3-d shape using the fastslam algorithm," in *Proc. AIAA Guidance, Navigation, and Control Conference (GNC)*, 2009.

[11] F. Aghili, M. Kuryllo, G. Okouneva, and C. English, "Robust vision-based pose estimation of moving objects for automated rendezvous & docking," in *Mechatronics and Automation (ICMA), 2010 International Conference on*, IEEE, 2010, pp. 305–311.

[12] C. Cocaud and T. Kubota, "Autonomous navigation near asteroids based on visual SLAM," in *Proceedings of the 23rd International Symposium on Space Flight Dynamics, Pasadena, California*, 2012.

[13] C. Vassallo, W. Tabib, and K. Peterson, "Orbital SLAM," in *12th Conference on Computer and Robot Vision (CRV)*, 2015, pp. 305–312. DOI: 10.1109/CRV.2015.47.

[14] C. Olson, R. P. Russell, and S. Bhaskaran, "Spin state estimation of tumbling small bodies," *The Journal of the Astronautical Sciences*, vol. 63, no. 2, pp. 124–157, 2016, ISSN: 2195-0571. DOI: 10.1007/s40295-015-0080-y.

[15] L. Carlone, R. Tron, K. Daniilidis, and F. Dellaert, "Initialization techniques for 3D SLAM: a survey on rotation estimation and its use in pose graph optimization," in *Robotics and Automation (ICRA), 2015 IEEE International Conference on*, IEEE, 2015, pp. 4597–4604.

[16] S. S. H. U. Gamage and J. Lasenby, "New least squares solutions for estimating the average centre of rotation and the axis of rotation," *Journal of biomechanics*, vol. 35, no. 1, pp. 87–93, 2002.

[17] J. Sola, D. Marquez, J.-M. Codol, and T. Vidal-Calleja, *An EKF-SLAM toolbox for MATLAB*, Available online: https://github.com/joansola/slamtb, 2009 (accessed on December 1, 2016).

[18] P. Pravec, A. W. Harris, and T. Michalowski, "Asteroid rotations," *Asteroids III*, vol. 113, 2002.